POLITECNICO DI TORINO
Repository ISTITUZIONALE

Enhanced Short-Time Thermal Transient Model and Testing Procedure for High Power Density Motors, Such as in Supercar Traction

Original
Enhanced Short-Time Thermal Transient Model and Testing Procedure for High Power Density Motors, Such as in Supercar Traction / Pescetto, P., Dilevrano, G., Stella, F., Pellegrino, G., Boglietti, A.. - In: IEEE OPEN JOURNAL OF INDUSTRY APPLICATIONS. - ISSN 2644-1241. - 6:(2025), pp. 391-402. [10.1109/ojia.2025.3579971]

Availability:
This version is available at: 11583/3008533 since: 2026-03-10T14:47:23Z

Publisher:
Institute of Electrical and Electronics Engineers Inc.

Published
DOI:10.1109/ojia.2025.3579971

Terms of use:

This article is made available under terms and conditions as specified in the corresponding bibliographic description in the repository

Publisher copyright

(Article begins on next page)

08 June 2026

IEEE Open Journal of
Industry Applications

Enhanced Short-Time Thermal Transient Model and Testing Procedure for High Power Density Motors, Such as in Supercar Traction

PAOLO PESCETTO (Member, IEEE), GAETANO DILEVRANO, FAUSTO STELLA (Member, IEEE), GIANMARIO PELLEGRINO (Fellow, IEEE), AND ALDO BOGLIETTI (Fellow, IEEE)

[1]Energy Department Galileo Ferraris, Politecnico di Torino, 10129 Torino, Italy

CORRESPONDING AUTHOR: PAOLO PESCETTO (e-mail: paolo.pescetto@polito.it).

The work was supported by the Power Electronics Innovation Center (PEIC) of Politecnico di Torino.

ABSTRACT The short-time thermal transient (STTT) test is an efficient and precise method for determining the winding thermal capacitance and winding-to-back-iron thermal resistance in ac motors. Traditionally validated for industrial motors, the STTT procedure involves a brief dc excitation with motor phases connected in series, followed by analysis using a first-order lumped parameter thermal network. However, for traction motor drives where phase terminals may be inaccessible, the standard all-in-series STTT procedure is not feasible. Moreover, in such highly loaded traction motors, the estimated thermal parameters are sensitive to dc excitation duration, making the first-order STTT model unsuitable. This article presents an STTT model of higher order along with an optimized testing sequence and data processing approach, extending the applicability of this method to traction and high-power-density motors. Experimental validation on two commercial supercar traction motors demonstrates the effectiveness of the proposed model and procedure, to be considered an upgrade of wider and more general validity of the existing first-order STTT method.

INDEX TERMS Lumped parameters thermal network, motor design, short time thermal transient, stator winding temperature, traction motor drives, thermal testing, thermal management.

NOMENCLATURE

R_{dc}	DC phase resistance.
θ_0, R_0	Ambient temperature and corresponding R_{dc}.
θ, $\Delta\theta$	Winding temperature and temperature rise respect to θ_0.
P_j, W	Joule loss and related dissipated energy.

I. INTRODUCTION

The design of high-performance electric machines, particularly for traction applications, is driven by stringent requirements for cost, efficiency, and power density [1], [2], [3]. This requires a multiphysics approach [4], combining magnetic, mechanical, and thermal design considerations [5], [6]. As the power density increases, advanced thermal management becomes critical, and liquid cooling is a key solution to minimize thermal impedance and accelerate thermal transients. While traditional motor drives testing focuses on magnetic characteristics [7], increasing attention is being paid to reliable methods for experimentally determining motor thermal properties [8], [9], [10]. Thermal models, based on finite element analysis (FEA) or lumped parameter thermal networks (LPTNs) [11], are essential for both the design and control stages [12], [13]. While FEA offers high accuracy, it demands detailed geometric and thermal property data, typically not available to the user. LPTNs provide a less detailed but computationally efficient approach for estimating temperature distributions with minimal computational effort. This work falls within the scope of LPTN models.

An accurate thermal LTPN must include the key parts of the motor, such as rotor and stator iron, windings, permanent magnets [14], [15]. Wrobel et al. [9] determined stator iron thermal capacitance using a dedicated adiabatic chamber and complex testing. Sciascera et al. [16] proposed an LPTN calibration based on uncertain parameters, such as convection coefficients, conductivity, and specific heat capacity, which

are often unknown to motor manufacturers and users. Other studies [17], [18] use regression and sensitivity analysis to extract the LPTN parameters, including iron thermal capacitance, by fitting the motor's thermal response. This requires numerous embedded thermistors and loss components segregation under ac or pulse with modulation (PWM) excitation, and may lead to nonphysical parameters, such as unrealistic resistances or capacitances. A similar approach was introduced in [19] based on a pseudorandom binary power loss excitation, but requiring a high number of embedded thermistors and a long execution time. Moreover, the impact of excitation and sampling frequency on the measured thermal parameters was not clearly established, resulting in a cumbersome calibration process for the excitation sequence.

The stator winding is a temperature vulnerable component, due to the strict temperature limit dictated by the isolation class [20]. The thermal properties of the winding conductors and the surrounding insulation material and stator iron are hardly computed analytically or numerically [16], [21], [22]. Despite some methods permit a comprehensive determination of the full thermal model of the machine, e.g., by temperature regression during a driving cycle [17], [18], a dedicated test is often devoted to the slot thermal parameters, given their crucial role for functional safety. In this context, the short-time thermal transient (STTT) test procedure was introduced in [23] and [24], for direct experimental evaluation of the winding thermal capacitance and resistance, referring to the first-order temperature model of general purpose induction motors with all the winding terminals accessible. This article shows that the STTT method fails describing the transient behavior of liquid cooled machines having low thermal inertia and high-performance cooling [25], [26]. In fact, the original STTT procedure [23], [24] assumes that the winding-to-iron thermal time constant is much faster than the iron-to-ambient heat exchange, which does not hold true for the liquid cooled motors under investigation. As a result, the STTT-derived winding thermal parameters are highly dependent on the test's duration.

A further drawback of the original STTT procedure is the related requirement of series connecting the motor phases implying the availability of their input and output terminals, normally not accessible in highly compact traction motors. A tentative solution was proposed in [27], still requiring the access to the star point of the machine.

A. ARTICLE CONTRIBUTIONS

This article presents an enhanced thermal model that addresses the outlined limitations of the method in [23]. By incorporating back iron temperature variation during the STTT test, the dependence of estimated thermal parameters on test duration is reduced by one order of magnitude.

In addition, three novel phase-to-phase testing methods are introduced, including the test sequence and data analysis. These techniques remove the necessity for output phase terminals or star point links, allowing them to be applicable to any practical application, irrespective of its star or delta winding arrangement. A comparative analysis of five testing configurations, including the three novel ones, is conducted to evaluate their accuracy and complexity. Practical challenges related to high-current, low-voltage dc excitation are addressed and resolved.

Furthermore, a sensitivity analysis is performed to assess the impact of different testing configurations and dc excitation durations on the estimated thermal parameters.

A further novel contribution of this work is the direct determination of stator iron thermal capacitance based on a simple and rapid test only involving dc power supply and voltage measurement, without requiring specialized equipment or parameters regression for a high-order LPTN.

Focusing on the stator thermal model, the proposed advanced STTT is not dependent on the rotor type. So, it is applicable to any type of ac machine, including internal or surface mounted permanent magnet synchronous motor (PMSM), induction motors, electrically excited synchronous motors, and switched reluctance motors.

The measured thermal parameters are valuable for fine-tuning thermal models assisting the design stage, in particular for accurately calibrating the thermal model of the slot, which is often one of the most complex parts. Furthermore, these parameters can be used for control purposes, enabling the calibration of advanced temperature observers for real-time thermal monitoring.

The proposed method is deemed highly effective and practical due to its simple test setup and reliable thermal parameter estimation. Its validity is substantiated by rigorous experimental validation on two supercar traction motors of varying sizes.

B. MOTORS UNDER TEST

The machines adopted for validating the proposal are two liquid cooled PMSMs of different size, labeled MUT1 and MUT2, designed for front and rear axles in supercar traction applications. As common for traction motors, the phase resistance is in the order of a few mΩ. In the embarkable version of the motors, only the three phase input terminals are accessible, which makes the original STTT procedure of [23] unfeasible. Both the prototypes under test have an additional neutral point wire to access the winding star point, for experimentation purposes. Due to manufacturing constraints, such additional wire has reduced cross-section and limited current capability, and the associated resistance is comparable to the resistance of one motor phase. Although not required for the STTT, each motor encapsulates three thermistors, each one located between two phases, which will be labeled *ab*, *bc*, and *ca*.

The design of these machines is proprietary, so every physical quantity in the article is normalized, and a detailed picture of the machines and the precise location of the thermistors could not be disclosed. The nominal thermal parameters are defined based on the finite element model of the machine, while the rated temperature rise is defined as the difference between the maximum winding temperature and the nominal inlet temperature of the coolant. Specifically, the nominal

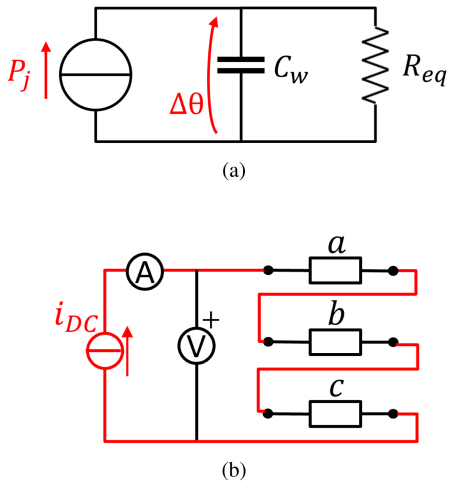

FIGURE 1. Original STTT procedure of [23]. (a) Equivalent LPTN, (b) DC identification test.

power of MUT1 and MUT2 is on the order of 200 and 350 kW, respectively. The isolation class of the coils defines the maximum winding temperature, and the nominal coolant temperature is 70°C, compliant with automotive standards. The nominal thermal capacitances of the winding and back iron are in the order of hundreds and thousands of J/°C, respectively.

II. ORIGINAL FIRST-ORDER LPTN STTT PROCEDURE

The STTT is a test procedure for estimating the slot thermal parameters of three-phase [23] or multiphase [24] electric motors. Referring to the first-order LPTN of Fig. 1(a), the winding thermal capacitance C_w, and the equivalent thermal resistance R_{eq} between the winding and the stator iron, including isolation and potting, are experimentally evaluated. The LPTN is designed in terms of winding temperature rise $\Delta\theta$ with respect to the ambient temperature θ_0. The stator iron temperature is considered constant at θ_0 during the test, so it is not included in the LPTN.

In [23], the three phases are series connected during the parameter identification test, as shown in Fig. 1(b). The test starts with the motor at a uniform ambient temperature θ_0. The series of the three phases is dc excited with a current i_{dc} compatible with the rms nominal current, producing a measurable temperature rise. The series connection ensures the uniform heating of the three phases. The imposed current i_{dc} and the voltage v_{dc} across the series of the three phases are measured, computing the winding resistance R_{dc}, Joule loss P_j, and estimated average winding temperature θ

$$R_{\text{dc}} = \frac{v_{\text{dc}}}{3 i_{\text{dc}}} \tag{1a}$$

$$P_j = v_{\text{dc}} \cdot i_{\text{dc}} \tag{1b}$$

$$\theta = \frac{R_{\text{dc}}}{R_0}\left(B_{Cu} + \theta_0\right) - B_{Cu} \tag{1c}$$

where R_0 is the winding resistance measured at θ_0, B_{Cu}=234.5°C is the inferred absolute temperature (or characteristic temperature) of the copper, and the temperatures θ and θ_0 are expressed in °C. Thanks to the dc excitation, the input power entirely converts into stator Joule loss, and the energy loss W can be computed as the time integral of P_j

$$W = \int_{t_0}^{t} P_j \, \mathrm{d}t \tag{2}$$

where t_0 is the time where the current step is imposed, associated with zero energy loss, i.e., $W(t_0) = 0$. The short duration of the dc excitation permits to assume that the system is initially adiabatic, so the heat exchange from the winding to its surroundings is negligible as well as the related thermal time constants. The adiabatic hypothesis is reasonable considering that the heat is first generated into the copper winding, and then transferred to the stator iron. The assumption holds for a minor initial rise of the winding temperature $\Delta\theta_{\text{st}}$, where "st" stands for "short transient"

$$\Delta\theta = \theta - \theta_0 < \Delta\theta_{\text{st}} \, . \tag{3}$$

Otherwise said, the initial heating of the copper was considered adiabatic within a temperature rise $\Delta\theta_{\text{st}}$ in the order of 3°C–5°C. As a consequence, W grows linearly with $\Delta\theta$ in this first part of the transient, and the energy versus temperature rise evolution $W(\Delta\theta)$ is approximated by a straight line $\hat{W}(\Delta\theta)$. The rate of change of the interpolating straight line estimates the winding thermal capacitance C_w

$$\hat{W}(\Delta\theta) = a \cdot \Delta\theta \quad \rightarrow \quad C_w = a \, . \tag{4}$$

The first-order LPTN, as depicted in Fig. 1(a), represents the stator winding during the STTT lapse, where the term C_w is "charged" by the Joule loss and the thermal resistance R_{eq} dissipates the heat to the surrounding iron. The evolution of the winding temperature rise is fitted *over time* with the analytical solution of the LPTN. This second fitting, carried over the STTT time horizon [0 Δt_{st}], permits estimating the R_{eq} based on the exponential time constant

$$\hat{\Delta\theta}(t) = P_j R_{\text{eq}}\left(1 - e^{-t/\tau_{\text{eq}}}\right) \quad \rightarrow \quad R_{\text{eq}} = \frac{\tau_{\text{eq}}}{C_w} \, . \tag{5}$$

The method assumes that the machine's thermal parameters remain constant within its typical operating temperature range, i.e., the LPTN is linear. So, while measured under dc conditions, the extracted thermal parameters are valid across real operating scenarios, including ac losses, iron losses, and PWM effects. DC test excitation simplifies and enhances the accuracy of measuring dissipated power, leading to more precise parameter determination. Moreover, the average winding temperature is retrieved only based on electrical measurement, thus not requiring embedded thermistors.

An example of STTT test based on [23] for a ventilated industrial motor is reported in Fig. 2. The figure reports in blue the dissipated energy and temperature rise characteristics, and in red the interpolations using (4) and (5), respectively. For this type of motors the first-order procedure is accurate, as the

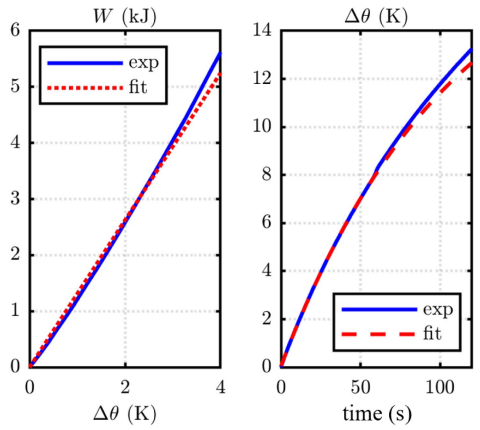

FIGURE 2. Example of STTT test results for an industrial motor drive according to [23]. Left: dissipated energy versus temperature rise; right: temperature rise versus time. Blue: measured data; red: interpolations with (4) and (5), respectively.

two fitting functions match the measurements, and the values of C_w and R_{eq} are robustly extracted. However, this test tends to fail for high-performance motors.

III. THREE- AND FOUR-TERMINAL IDENTIFICATION TESTS AND DATA PROCESSING

The motors under test presents several peculiarities making the traditional STTT procedure unfeasible (the output phase terminals are not accessible) and unreliable (the first-order model fails). This section describes how this work addresses the STTT identification test, with the goal of retrieving the thermal parameters C_w and R_{eq}. Five alternative testing configurations are proposed for such high-performance drives where the first-order STTT fails.

A. CONFIGURATION 1: PARALLEL PHASE CONNECTION

Series connection reported in Fig. 1(b) is not feasible in embarkable traction motors, and in general to ac motors with three phase terminals. As said in Section I-B, in the prototypes under test, the star point is made accessible through an additional connection having a resistance R_{add} compatible with the phase resistance, due to the small gauge of the additional wire. The first alternative to the all-series connection is the parallel connection of Fig. 3(a). This is still heating the three phases evenly, but with the following three downsides:

1) controlling a high dc current on a very small resistance;
2) the series resistance R_{add} must be accounted for;
3) an eventual mismatch in the resistance of the three phases causes severe unbalance in the current and loss distribution among the phases.

About point 1), the dc current generator must provide three times the rated rms phase current of the machine, which is in the order of hundreds of A, to a load of a few mΩ or less, seen the paralleled phases. For example, a current between 300 and 700 A must be provided with a voltage between 1 and 5 V. The stable and accurate control of the dc turns out

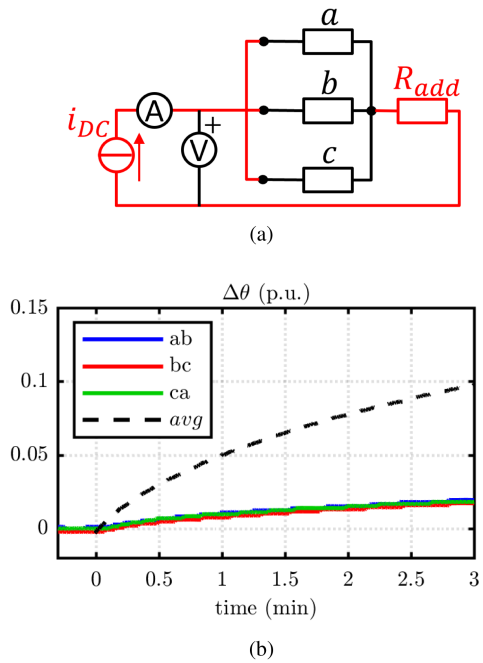

FIGURE 3. MUT2: STTT identification test according to configuration 1. (a) Parallel phases with additional resistance in series. (b) Estimated winding temperature (dashed black) and winding thermistors (colored lines). The presence of R_{add} harms the accuracy of the test.

to be a hard challenge for most of dc sources, and requires specialized equipment. Dealing with point 2), the term R_{add} is not related to the winding temperature and invalidates its estimation through (1c). About 3), being R_s in the order of a few mΩ, a relevant resistance mismatch between the phases is easily produced, e.g., due to different contact resistance or cable length for the connection with the dc supply.

The parallel connection was tested on MUT2, with the results reported in Fig. 3(b). The figure reports in black the average winding temperature, estimated with (1c), together with the measurements coming from the winding embedded thermistors of the prototype. The influence of R_{add} is clearly visible, as the average temperature estimated with (1c) is unrealistically larger than any measured temperature. This is explained considering that the additional wire adopted for accessing the star point, having a reduced section and three times the phase current, was considerably hotter than the winding, thus deviating the average temperature estimate. Considering these issues, *the parallel connection of Fig. 3(a) was dismissed*.

B. CONFIGURATION 2: DUAL SUPPLY CONNECTION

A second option is to use two dc current sources, connected as in Fig. 4(a). The first dc source, exciting phases *a* and *b*, permits measuring the phase resistance, loss, and estimated temperature rise. The second dc source excites the third phase through the star point connection with the exact same current, to maintain the thermal homogeneity of the three phases. If compared to the parallel configuration, this topology requires

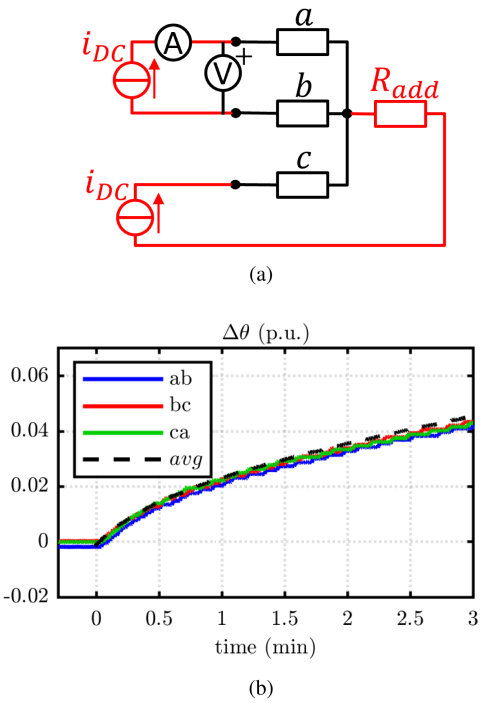

FIGURE 4. MUT2: STTT identification test according to configuration 2. (a) Dual dc supply for compensation of R_{add}. (b) Estimated average winding temperature (black dashed) and winding thermistors (colored lines).

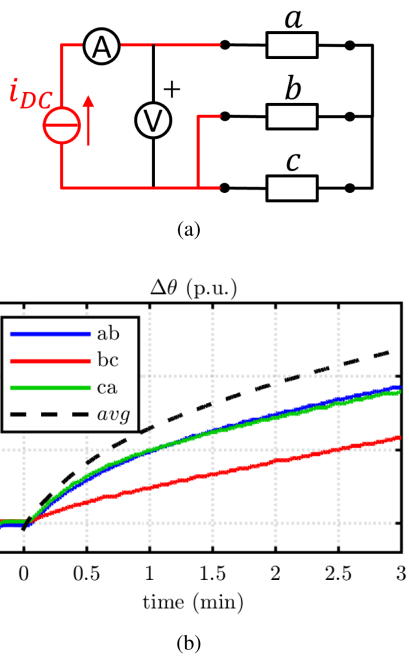

FIGURE 5. MUT2: STTT identification test according to configuration 3. (a) Two parallel phases connection. (b) Estimated average winding temperature (black dashed) and winding thermistors (colored lines).

two dc sources with only 1/3 of the current rating to achieve the same temperature rise, thus simplifying the hardware requirements. Moreover, the weak connection to the star point needs to sustain the phase current i_{dc}, instead of $3i_{\mathrm{dc}}$. Most importantly, the measurement branch only includes the phases a and b, excluding the extraneous term R_{add}. This allows for an independent estimation of the winding temperature via (1c). The resistance and dissipated power equations are modified as

$$R_{\mathrm{dc}} = \frac{v_{\mathrm{dc}}}{2i_{\mathrm{dc}}} \tag{6a}$$

$$P_j = \frac{3}{2} v_{\mathrm{dc}} \cdot i_{\mathrm{dc}} \,. \tag{6b}$$

The temperature evolution during the test is reported in Fig 4(b). As can be seen, the estimated average winding temperature (black line) is realistic, as it well tracks the temperatures measured by the embedded thermistors. The layout of Fig. 4(a) proved to be accurate in [27]. Still, at least a weak access to the star point is required.

C. CONFIGURATION 3: ONE PHASE IN, TWO PHASE OUT CONNECTION

In this configuration, as illustrated in Fig. 5(a), one of the phases is supplied with the full dc and the other two with half of that. This is the first attempt at performing the STTT without any access to the winding star point. It permits to measure the average resistance of the three phases, although the corresponding average temperature is not representative of any of the phases individually

$$R_{\mathrm{dc}} = \frac{3v_{\mathrm{dc}}}{2i_{\mathrm{dc}}} \,. \tag{7}$$

Although this solution does not require access to the star center, the thermal distribution is asymmetric for two reasons: 1) due to the difference between the phase supplied with full current and the other two, and 2) due to a possible imbalance of the two phases in parallel. As expected, Fig. 5(b) shows that the thermistor *bc* placed between the two phases in parallel heats more slowly than those involving the phase *a*, which is supplied with full current. Moreover, the estimated average temperature cannot be associated with any of the three phases. Since this solution has not yielded significant results, *it will not be considered in the subsequent sections*.

D. CONFIGURATION 4: PHASE-TO-PHASE CONNECTION

In this test configuration, as illustrated in Fig. 6(a), the machine is again heated asymmetrically as the third phase is not supplied with any power. However, the two powered phases heat homogeneously and with the same dynamics. It is thus possible to monitor their resistance and average temperature

$$R_{\mathrm{dc}} = \frac{v_{\mathrm{dc}}}{2i_{\mathrm{dc}}} \,. \tag{8}$$

The nonsupplied phase remains colder. The average temperature [see Fig. 6(b)] shows a reasonable trend: the phases *a* and *c* heat up homogeneously, and their average temperature well corresponds to the thermistor *ca* placed between them.

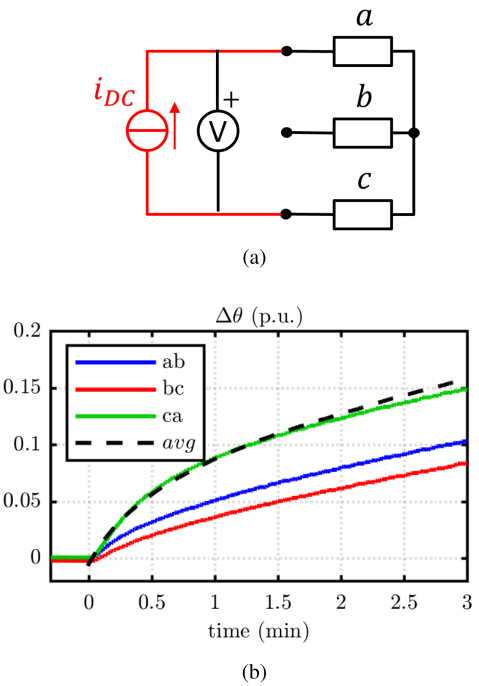

FIGURE 6. MUT2: STTT identification test according to configuration 4. (a) Phase-to-phase connection. (b) Estimated average winding temperature (black dashed) and winding thermistors (colored lines).

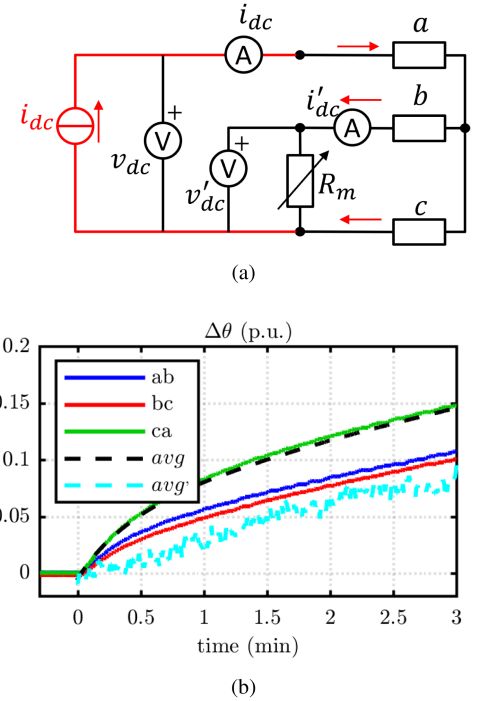

FIGURE 7. MUT2: STTT identification test in configuration 5. (a) Phase-to-phase connection and third phase monitored. (b) Estimated average winding temperatures (black and light blue) and thermistors (solid lines).

The phase b remains colder, as confirmed by the thermistors ab and bc. In this configuration, the power losses generated in the phases a and c are partially dissipated directly through the stator iron and partially through the "cold" phase b. Therefore, a lower R_{eq} would be evaluated by the STTT procedure, and the thermal transient is faster with respect to the cases of configuration 2, where all three phases are excited. Still, with a proper postprocessing of the measurement, this configuration remains interesting for determining the thermal parameters without any access to the star center. Further details will be provided in Section IV-C.

E. CONFIGURATION 5: PHASE-TO-PHASE CONNECTION AND THIRD PHASE MONITORED

Configuration 4 lacks information on the nonexcited phase. This is overcome by the setup proposed in Fig. 7(a), where a calibrated resistance R_m is added to the phase-to-phase configuration to monitor the third-phase temperature. The value of R_m is chosen to be much higher than the phase resistance, thus forcing almost all the current of the dc source to flow into phase c ($\approx$0.95 i_{dc}), leaving minimal current in phase b ($\approx$0.05 i_{dc}). From a thermal perspective, configuration 4 (phase-to-phase power supply) is replicated, as the Joule losses in phase b are negligible. This is confirmed by the embedded thermistors, measuring almost the same thermal transient in Figs. 6(b) and 7(b). The R_m branch is intended for monitoring the resistance variation of the phase b. The resistance R_{dc} and average temperature θ of the powered phases are distinguished from the resistance R'_{dc} and temperature θ' of the not supplied phase

$$R_{s,a} = R_{s,c} = R_{\text{dc}} = \frac{v_{\text{dc}}}{2i_{\text{dc}} - i'_{\text{dc}}} \tag{9a}$$

$$R_{s,b} = R'_{\text{dc}} = \frac{v'_{\text{dc}} - R_{\text{dc}}(i_{\text{dc}} - i'_{\text{dc}})}{i'_{\text{dc}}}\,. \tag{9b}$$

The two average temperatures are reported in dashed lines in Fig. 7(b), in black and light blue, respectively. As per configuration 4, the heat is partially dissipated directly through the back iron and partially through the nonexcited phase. The temperature monitoring of the phase b permits to distinguish the two contributions, as will be discussed in Section IV-C.

IV. SECOND-ORDER IMPROVED MODEL AND PARAMETERS EXTRACTION

In [23], the duration of the initial thermal transient, i.e., the adiabatic temperature rise range $\Delta\theta_{\text{st}}$ and time interval Δt_{st} where the system follows a first-order transient, was easy to be chosen arbitrarily. The technique showed its robustness for industrial motors, forgiving even large temperature and time interval variations. Conversely, compact and highly loaded traction machines are designed for an extremely high rate of heat extraction. The fundamental hypothesis of the STTT, i.e., that the initial part of the thermal transient is adiabatic, tends to fail. In particular the function $W(\Delta\theta)$ immediately starts growing nonlinearly, and cannot be approximated with a straight line to determine the thermal capacitance C_w with

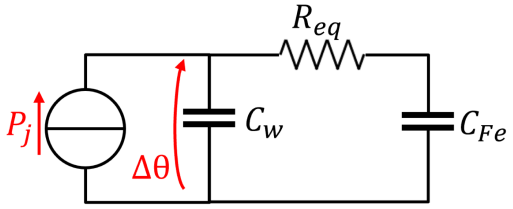

FIGURE 8. Proposed LPTN for STTT procedure in configuration 2.

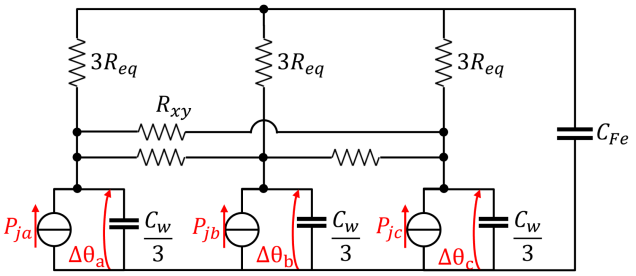

FIGURE 9. Proposed generalized three-phase LPTN for STTT procedure with asymmetrical configurations 4 and 5.

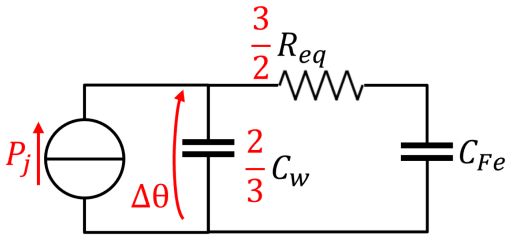

FIGURE 10. Approximated LPTN for STTT procedure in configuration 4.

(4). Similarly, the temperature evolution is badly described by a first-order thermal transient, impeding the adoption of (5) for determining $\hat{\Delta\theta}(t)$ and R_{eq}. This is confirmed by the thermal transients measured with the configurations described above.

To solve this issue, two actions were adopted as follows.

1) The hypothesis of the initial adiabatic transient was moved from the winding alone to the full stator.
2) The iron capacitance was introduced in the LPTN, leading to a second-order system.

A. DISSIPATED ENERGY AND THERMAL CAPACITANCE

Based on the first point, i.e., a nonadiabatic winding during the STTT, a nonlinear $W(\Delta\theta)$ function is assumed, and approximated with its third-order Taylor series expansion

$$\hat{W}(\Delta\theta) = a_3 \cdot \Delta\theta^3 + a_2 \cdot \Delta\theta^2 + a_1 \cdot \Delta\theta \ . \tag{10}$$

The initial derivative of $W(\Delta\theta)$ still corresponds to the winding thermal capacitance C_w, and can be analytically determined as

$$\left.\frac{\mathrm{d}\hat{W}}{\mathrm{d}\Delta\theta}\right|_{\Delta\theta=0} = a_1 \quad \rightarrow \quad C_w = a_1 \ . \tag{11}$$

This method applies for all the considered STTT configurations 2, 4, and 5. As said, configurations 1 and 3 proved to be inaccurate, and will not be further discussed.

B. EQUIVALENT LPTN IN CONFIGURATION 2

Dealing with the second-order LPTN, with the STTT executed in configuration 2, the iron thermal capacitance C_{Fe} is introduced, as shown in Fig. 8, to include the nonnegligible temperature rise of the stator iron. Still, the stator is considered adiabatic during the STTT, as the heat dissipation from the iron to the ambient (or to the coolant) is not considered, being negligible in the initial part of the thermal transient. The temperature rise is interpolated through the analytical solution of the LPTN in Fig. 4(a), permitting to estimate R_{eq} from the time constant τ_{eq}

$$\hat{\Delta\theta}(t) = \frac{P_j}{C_w + C_{Fe}} t + P_j R_{\text{eq}} \frac{C_{Fe}^2}{(C_w + C_{Fe})^2} \left(1 - e^{-t/\tau'_{\text{eq}}}\right) \tag{12a}$$

$$\tau'_{\text{eq}} = \frac{C_w C_{Fe}}{C_w + C_{Fe}} \cdot R_{\text{eq}} \approx C_w \cdot R_{\text{eq}} \ . \tag{12b}$$

In addition, this interpolation permits estimating the thermal capacitance of the stator iron, extracted from the linear coefficient $\frac{P_j}{C_w + C_{Fe}}$. Such C_{Fe} estimation resulted consistent with the analytical calculation based on the stator geometry. It should be noted that the original procedure in [23] does not provide any information about C_{Fe}.

C. EQUIVALENT LPTN IN CONFIGURATIONS 4 AND 5

In the cases where the phases are not equally excited, as in the single-phase configurations 4 and 5, the temperature difference between the three phases must be considered. A generalized LPTN is proposed in Fig. 9. Each phase is associated with 1/3 of the winding capacitance $C_w/3$ and three times the winding-to-iron resistance $3R_{\text{eq}}$. Different Joule losses P_{ja}, P_{jb}, and P_{jc} are associated with each phase, depending on the excitation and testing configuration. Specifically for the configurations 4 and 5, $P_{ja} = P_{jc} = P_j/2$ and $P_{jb} = 0$. The phase-to-phase thermal resistance R_{xy} is introduced to model the heat dissipation through the nonexcited phase. In the case of symmetrical supply ($P_{ja} = P_{jb} = P_{jc} = P_j/3$) the three phase temperatures are equal, and the LPTN collapses to the one in Fig. 8.

In the case of STTT executed in configuration 4, no information is given about the temperature rise in phase b. A suitable approximation can be assumed by neglecting the thermal coupling between the phases ($R_{xy} \rightarrow \infty$). Under this assumption, the heat transferred to the disconnected phase can be neglected, and the system reduces to the approximated LPTN reported in Fig. 10. Based on this network, the winding thermal capacitance and the resistance R_{eq} can be retrieved following the same procedure described in Section III-B, i.e., from (11) and (12). This corresponds to computing the thermal parameters relative to two phases; the thermal parameters

FIGURE 11. Test bench for the experimental validation.

of the full stator are computed applying a rescaling factor of 2/3, as indicated in Fig. 10.

Since the heat dissipation through phase b was neglected, this approach leads to underestimating R_{eq}. The entity of this underestimation depends on the thermal promiscuity of the three phases, and so on the winding configuration being, for example, a concentrated or distributed winding stator. The entity of the underestimation could be corrected as follows:

1) based on thermal FEA;
2) based on experience on similar motors;
3) performing the STTT in configuration 5.

In this latter case, the equivalent thermal resistance is still computed from the thermal time constant and capacitance, but corrected to compensate for the heat transferred through the nonexcited phase

$$R_{\mathrm{eq}} = \frac{\tau'_{\mathrm{eq}}}{C_w} \cdot \frac{\overline{v}_{\mathrm{dc}}\overline{i}_{\mathrm{dc}} + \overline{v}'_{\mathrm{dc}}\overline{i}'_{\mathrm{dc}}}{\overline{v}_{\mathrm{dc}} i_{\mathrm{dc}}} \tag{13}$$

where $\overline{v}_{\mathrm{dc}}$, $\overline{i}_{\mathrm{dc}}$, $\overline{v}'_{\mathrm{dc}}$, and $\overline{i}'_{\mathrm{dc}}$ are the voltages and currents measured in configuration 5 averaged over the time Δt_{st}.

V. EXPERIMENTAL RESULTS

The proposal was validated on two high-performance traction motors. Fig. 11 depicts the test bench. All the five proposed configurations were tested. The results are reported in Figs. 3(b), 4(b), 5(b), 6(b), and 7(b), respectively, all referred to the MUT2. Per each test, although only the initial thermal transient is of interest for the STTT procedure, the dc excitation was maintained for a largely longer time, to evaluate the effect of $\Delta\theta_{\mathrm{st}}$ and Δt_{st} calibration.

A. SENSITIVITY TO $\Delta\theta_{\mathrm{st}}$ AND Δt_{st} CALIBRATION

This section investigates the effect of the fitting intervals $\Delta\theta_{\mathrm{st}}$ and Δt_{st} on the measured thermal parameters. Fig. 12 reports in blue the experimentally measured energy variation versus

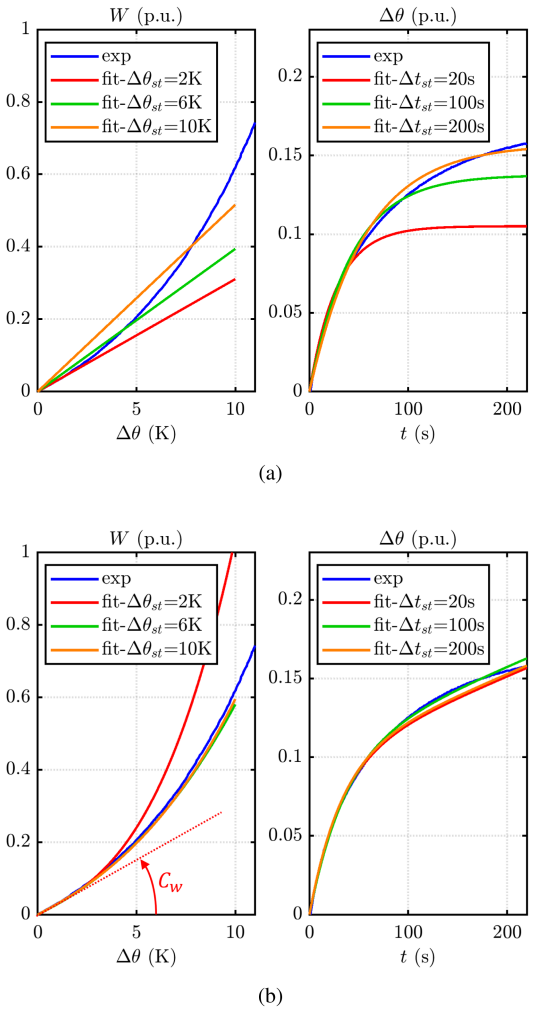

FIGURE 12. STTT results. (a) Method in [23]: $W(\Delta\theta)$ interpolated with (4) and $\Delta\theta(t)$ interpolated with (5). (b) Proposed configuration 2: $W(\Delta\theta)$ interpolated with (11) and $\Delta\theta(t)$ interpolated with (12).

temperature rise and the temperature rise versus time curves, with the STTT executed in configuration 2 on the MUT1. In Fig. 12(a), data were interpolated as in [23] using (4) and (5), under different fitting domains, with $\Delta\theta_{\mathrm{st}}$ spanning from 2 to 10 K and Δt_{st} from 10 to 200 s. As the estimate of C_w is the slope of the interpolating straight line (4), this strongly depends on the adopted $\Delta\theta_{\mathrm{st}}$. Also, based on (5), the R_{eq} estimate derives from the time constant of the first-order temperature rise fit, which considerably varies with the choice of the time horizon used for the interpolation Δt_{st}. This confirms that the existing STTT procedure [23] leads to unreliable estimation of the STTT parameters.

The same set of measurements was analyzed with the proposed procedure, i.e., using (11) and (12), under the same ranges of fitting domains. The results are reported in Fig. 12(b). In this case, C_w is the initial slope of the fitting function $\hat{W}(\Delta\theta)$. As can be noted, the thermal capacitance is consistently evaluated independently by the interpolation domain. Moreover, almost the same thermal time constant

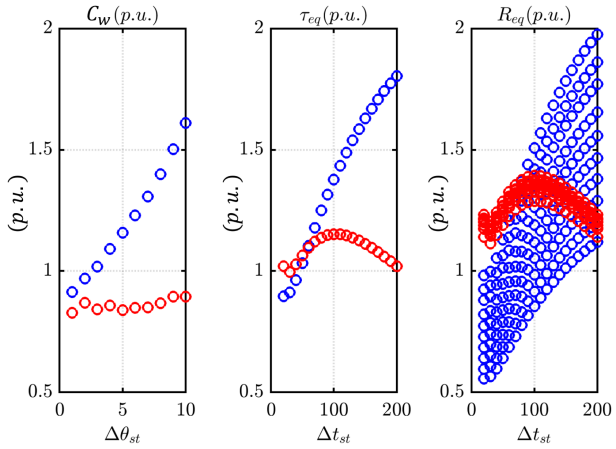

FIGURE 13. MUT1: Dispersion of the estimated parameters on varying $\Delta\theta_{st}$ and Δt_{st}. Blue: method in [23]; red: proposed analysis.

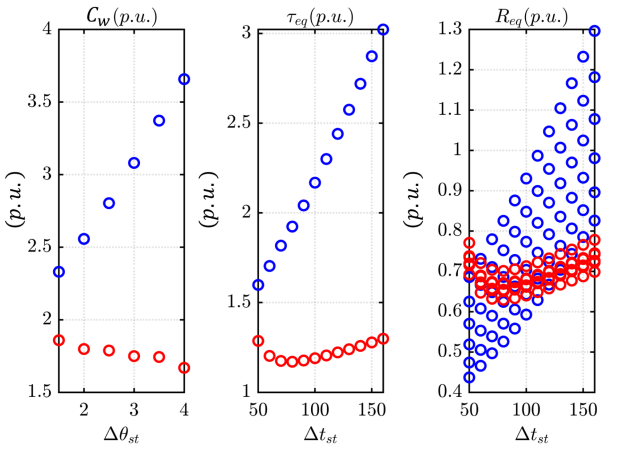

FIGURE 14. MUT2: Dispersion of the estimated parameters on varying $\Delta\theta_{st}$ and Δt_{st}. Blue: method in [23]; red: proposed analysis.

TABLE 1. Mean Value (μ) and Standard Deviation (σ) of the Measured Thermal Parameter in the Original and Proposed STTT Procedures

	μ		σ	
	[23]	Proposed	[23]	Proposed
C_w (p.u.)	1.220	0.859	0.222	0.021
τ_{eq} (p.u.)	1.389	1.091	0.299	0.051
R_{eq} (p.u.)	1.177	1.272	0.331	0.067

(and so R_{eq}) is estimated on the $\Delta\theta$ evolution, regardless of the calibration of $\Delta\theta_{st}$.

The thermal parameters obtained with [23] and with the proposed procedure are reported in Fig. 13, in blue and red dots, respectively, while Table 1 presents their average values μ and dispersion σ. The proposed method offers a significant improvement in parameter sensitivity compared to the original procedure, reducing the standard deviation by an order of magnitude when compared to the method in [23].

The same sensitivity analysis was conducted for the MUT2, again varying the time interval and the maximum temperature rise. It should be remembered that MUT2 is significantly larger in power ratings and volume respect to MUT1. The results are illustrated in Fig. 14, and are in line with those obtained for MUT1. This confirms that the sensitivity to the calibration is significantly reduced using the proposed procedure regardless the size of the machine.

B. EFFECT OF TEST CONFIGURATIONS

The impact of testing configurations on the estimated thermal parameters is investigated, again referring to MUT2. The results are depicted in Fig. 15, referring to the STTT executed in configuration 2 (red dots), configuration 4 (green dots), and configuration 5 (black dots).

It can be noted that the phase-to-phase power supply in configuration 4 allows for a correct estimation of the winding's thermal capacity and a limited but systematic underestimation of the equivalent thermal resistance, as expected. As mentioned, this systematic discrepancy could be compensated

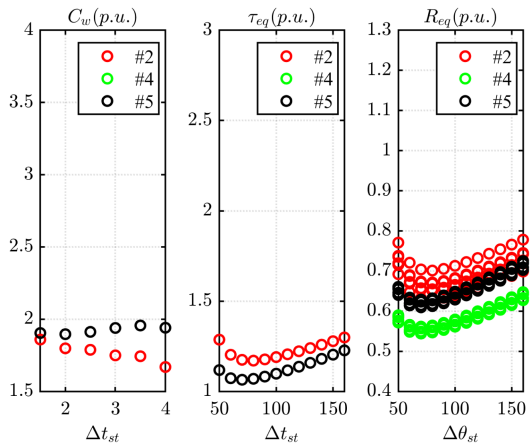

FIGURE 15. MUT2: Dispersion of the estimated parameters on varying $\Delta\theta_{st}$ and Δt_{st}. Red: configuration 2; green: configuration 4; black: configuration 5.

either through corrective coefficients, determined based on experience or on FEA, or through the temperature monitoring of the phase *b* (configuration 5).

The results obtained in configuration 5 show a minor deviation respect to the thermal parameters measured in configuration 2. This demonstrates the effective capability of the proposed method to extract the stator thermal parameters from a single-phase dc excitation of the machine, thus without requiring access to the star point.

C. ESTIMATION OF IRON THERMAL CAPACITANCE

The STTT in configurations 4 and 5 permit the estimation of the iron thermal capacitance, retrieved from the linear coefficient in (12). The sensitivity of C_{Fe} estimation on varying Δt_{st} is investigated in Fig. 16. As can be seen, the estimated C_{Fe} is weakly dependent on the duration of the STTT test, and coherent with the FEA analysis. It should be remarked that the original STTT procedure in [23] does not permit estimating the iron capacitance.

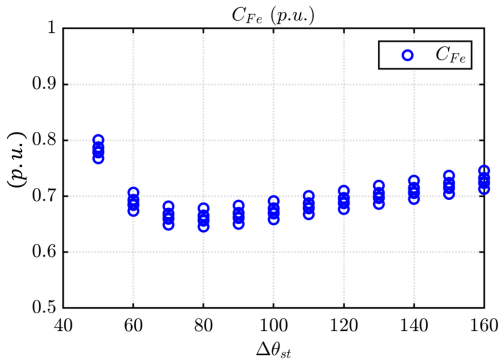

FIGURE 16. MUT2: Dispersion of the estimated C_{Fe} on varying Δt_{st} in configuration 4.

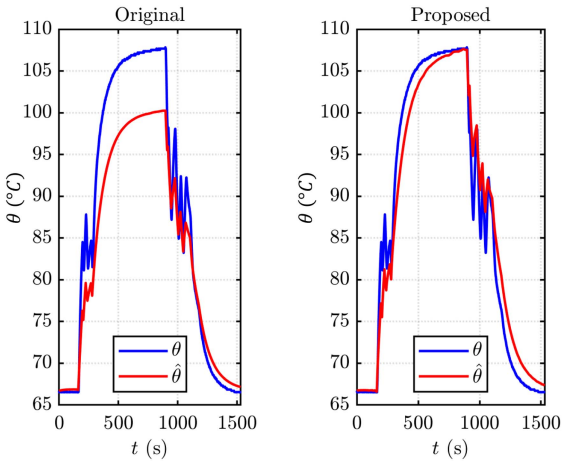

FIGURE 17. Example of temperature prediction through a LPTN calibrated with [23] (left) and with the proposed analysis (right).

D. APPLICATION EXAMPLE: REAL-TIME TEMPERATURE OBSERVER

Finally, an application example is given in Fig. 17, where the parameters C_w and R_{th} extracted from the STTT were adopted for calibrating an advanced hotspot temperature observer. Both the MUTs present a hotspot, which location has been determined in collaboration with the carmaker. For these compact motors used in hypercar traction, it is not feasible to place a thermistor directly at the winding hotspot, so this temperature is estimated through the real-time observer. Still, a thermocouple was embedded in both prototypes for development and testing purposes.

The real-time hotspot temperature observer presented in [28] was employed. While many temperature observers in the literature face significant calibration challenges, a key advantage of [28] is that the observer can be fully calibrated using the STTT parameters C_w, C_{Fe}, and R_{eq}. The observer relies on the machine's loss estimates and a thermistor placed at the only accessible point of the winding, near the inverter connection and thermally distant from the hotspot. The results are reported in Fig 17, showing the measured and estimated hotspot temperatures in blue and red lines, respectively, with the motor operating under a complex load cycle. The plot compares the temperature estimate obtained while calibrating the temperature observer based on [23] (left subplot) and with the proposed procedure (right subplot). The comparison clearly illustrates the impact of the observer's calibration on the accuracy of the predicted hotspot temperature and demonstrates the superiority of the proposed method.

VI. CONCLUSION

The STTT model permits to determine the thermal capacitance of the stator winding and the equivalent thermal resistance between the winding and the stator iron, which are key building blocks for an accurate LPTN transient thermal model of an ac machine. This work proposed and validated an improved STTT testing procedure for high-performance, liquid cooled motor drives, without requiring the access to the windings output terminals. A novel experimental setup is proposed, to guarantee the thermal symmetry of the motor, but it still needs at least a weak connection with the star point. Two alternative phase-to-phase configurations are also proposed, permitting the retrieval of the three-phase thermal parameters without any access to the star point. Furthermore, per each of the novel testing configurations, a newly proposed second-order LPTN and postprocessing method are developed to accurately retrieve the winding thermal parameters independently from the domain of the thermal analysis, dropping the adiabatic hypothesis of previous methods. In addition, the proposal permits estimating the stator iron thermal capacitance based on a rapid test only involving dc power supply and voltage measurement, without specialized equipment. The proposed STTT approach is validated with experiments on two synchronous high-performance motors for supercars traction, demonstrating its accuracy and robustness regardless the size of the machine, the duration of test excitation and testing configuration.

The proposed method can be commercially exploited for thermal characterization of machine prototypes embedding star-point connection, targeting a refinement of the design procedures and thermal models, as well as for fast end-of-line thermal testing in applications where the star point is not accessible.

REFERENCES

[1] F. Momen, K. Rahman, and Y. Son, "Electrical propulsion system design of chevrolet bolt battery electric vehicle," *IEEE Trans. Ind. Appl.*, vol. 55, no. 1, pp. 376–384, Jan./Feb. 2019.

[2] W. Jiang and T. M. Jahns, "Coupled electromagnetic–thermal analysis of electric machines including transient operation based on finite-element techniques," *IEEE Trans. Ind. Appl.*, vol. 51, no. 2, pp. 1880–1889, Mar./Apr. 2015.

[3] A. Krings and C. Monissen, "Review and trends in electric traction motors for battery electric and hybrid vehicles," in *Proc. 2020 Int. Conf. Elect. Machines*, 2020, pp. 1807–1813.

[4] N. Rivière, M. Stokmaier, and J. Goss, "An innovative multi-objective optimization approach for the multiphysics design of electrical machines," in *Proc. 2020 IEEE Transp. Electrific. Conf. Expo*, 2020, pp. 691–696.

[5] S. Li, Y. Li, W. Choi, and B. Sarlioglu, "High-speed electric machines: Challenges and design considerations," *IEEE Trans. Transport. Electrific.*, vol. 2, no. 1, pp. 2–13, Mar. 2016.
[6] R. Leuzzi, P. Cagnetta, S. Ferrari, P. Pescetto, G. Pellegrino, and F. Cupertino, "Transient overload characteristics of PM-assisted synchronous reluctance machines, including sensorless control feasibility," *IEEE Trans. Ind. Appl.*, vol. 55, no. 3, pp. 2637–2648, May/Jun. 2019.
[7] A. Allca-Pekarovic, P. J. Kollmeyer, A. Forsyth, and A. Emadi, "Experimental characterization and modeling of a yasa p400 axial flux PM traction machine for electric vehicles," in *Proc. 2022 IEEE Transp. Electrific. Conf. Expo*, 2022, pp. 433–438.
[8] Y. Gai et al., "Cooling of automotive traction motors: Schemes, examples, and computation methods," *IEEE Trans. Ind. Electron.*, vol. 66, no. 3, pp. 1681–1692, Mar. 2019.
[9] R. Wrobel, B. Mecrow, and M. Benarous, "Thermal evaluation of a short-operating-duty dual-lane fault-tolerant actuator for aerospace applications," *IEEE Trans. Ind. Appl.*, vol. 59, no. 4, pp. 4083–4094, Jul./Aug. 2023.
[10] N. Simpson, R. Wrobel, and P. H. Mellor, "Estimation of equivalent thermal parameters of impregnated electrical windings," *IEEE Trans. Ind. Appl.*, vol. 49, no. 6, pp. 2505–2515, Nov./Dec. 2013.
[11] C. Kral, A. Haumer, M. Haigis, H. Lang, and H. Kapeller, "Comparison of a CFD analysis and a thermal equivalent circuit model of a tefc induction machine with measurements," *IEEE Trans. Energy Convers.*, vol. 24, no. 4, pp. 809–818, Dec. 2009.
[12] O. Wallscheid, "Thermal monitoring of electric motors: State-of-the-art review and future challenges," *IEEE Open J. Ind. Appl.*, vol. 2, pp. 204–223, 2021.
[13] N. Z. Popov, S. N. Vukosavic, and E. Levi, "Motor temperature monitoring based on impedance estimation at PWM frequencies," *IEEE Trans. Energy Convers.*, vol. 29, no. 1, pp. 215–223, Mar. 2014.
[14] V. Madonna, P. Giangrande, L. Lusuardi, A. Cavallini, C. Gerada, and M. Galea, "Thermal overload and insulation aging of short duty cycle, aerospace motors," *IEEE Trans. Ind. Electron.*, vol. 67, no. 4, pp. 2618–2629, Apr. 2020.
[15] L. Jin, Y. Mao, X. Wang, L. Lu, and Z. Wang, "A model-based and data-driven integrated temperature estimation method for PMSM," *IEEE Trans. Power Electron.*, vol. 39, no. 7, pp. 8553–8561, Jul. 2024.
[16] C. Sciascera, P. Giangrande, L. Papini, C. Gerada, and M. Galea, "Analytical thermal model for fast stator winding temperature prediction," *IEEE Trans. Ind. Electron.*, vol. 64, no. 8, pp. 6116–6126, Aug. 2017.
[17] O. Wallscheid and J. Böcker, "Global identification of a low-order lumped-parameter thermal network for permanent magnet synchronous motors," *IEEE Trans. Energy Convers.*, vol. 31, no. 1, pp. 354–365, Jan. 2016.
[18] J. García Urbieta, B. Rodríguez, A. J. Rodríguez, P. Díaz, S. Armentia, and F. González, "Sensitivity analysis of lumped-parameter thermal networks for the experimental calibration of emotor models," *IEEE Trans. Transport. Electrific.*, vol. 10, no. 3, pp. 6210–6220, Sep. 2024.
[19] N. Krause, D. Sossong, and I. P. Brown, "Greybox thermal parameter identification of electric machine stators," in *Proc. 2024 IEEE Energy Convers. Congr. Expo.*, 2024, pp. 5447–5454.
[20] H. Xu, K. Lin, C. Ehrenpreis, G. Roux, and R. W. De Doncker, "Thermal modeling of electrical machines with advanced fluid cooling," in *Proc. 19th IEEE Intersociety Conf. Thermal Thermomechanical Phenomena Electron. Syst.*, 2020, pp. 491–496.
[21] K. Bersch, S. Nuzzo, P. H. Connor, C. N. Eastwick, R. Rolston, and M. Galea, "Thermal and electromagnetic stator vent design optimisation for synchronous generators," *IEEE Trans. Energy Convers.*, vol. 36, no. 1, pp. 207–217, Mar. 2021.
[22] M. C. Kulan and N. J. Baker, "Development of a thermal equivalent circuit to quantify the effect of thermal paste on heat flow through a permanent magnet alternator," *IEEE Trans. Ind. Appl.*, vol. 55, no. 2, pp. 1261–1271, Mar./Apr. 2019.
[23] A. Boglietti, E. Carpaneto, M. Cossale, and S. Vaschetto, "Stator-winding thermal models for short-time thermal transients: Definition and validation," *IEEE Trans. Ind. Electron.*, vol. 63, no. 5, pp. 2713–2721, May 2016.
[24] P. Pescetto, S. Ferrari, G. Pellegrino, E. Carpaneto, and A. Boglietti, "Winding thermal modeling and parameters identification for multithree phase machines based on short-time transient tests," *IEEE Trans. Ind. Appl.*, vol. 56, no. 3, pp. 2472–2480, May/Jun. 2020.
[25] J. Goss, R. Wrobel, P. Mellor, and D. Staton, "The design of ac permanent magnet motors for electric vehicles: A design methodology," in *Proc. Int. Elect. Mach. Drives Conf.*, 2013, pp. 871–878, doi: 10.1109/IEMDC.2013.6556200.
[26] P. Roy et al., "An algorithm for effective design and performance investigation of active cooling system for required temperature and torque of PM traction motor," *IEEE Trans. Magn.*, vol. 57, no. 2, Feb. 2021, Art. no. 8201507.
[27] P. Pescetto, G. Dilevrano, G. Pellegrino, and A. Boglietti, "Improved short time thermal transient model and testing procedure for high power density motors," in *Proc. 2023 IEEE Int. Electric Machines Drives Conf.*, 2023, pp. 1–6.
[28] P. Pescetto, G. Dilevrano, G. Pellegrino, and A. Boglietti, "LPTN-based real-time stator hotspot temperature estimation for enhanced thermal management in high-performance PMSMs," *IEEE Access*, vol. 13, pp. 103166–103177, 2025, doi: 10.1109/ACCESS.2025.3578802.

PAOLO PESCETTO (Member, IEEE) received the Ph.D. (Hons.) degree in electrical, electronical and communication engineering from Politecnico di Torino, Turin, Italy, in 2019.

Since fall 2019, he has been a Researcher and Tenure-Track Lecturer with the Energy Department of Politecnico di Torino. He is currently an Assistant Professor with Politecnico di Torino. He is a Member of the Power Electronics Innovation Center, Politecnico di Torino. In 2014, he was an Erasmus Student with the Norwegian University of Science and Technology, Trondheim, Norway. He has authored or coauthored more than 50 scientific works, with more than 15 IEEE journal papers and five patents. His research interests include synchronous motor drives, sensorless control, self-commissioning techniques, thermal models, and integrated battery chargers for EVs.

Dr. Pescetto has been the Vice Chair of the IEEE IA/IE/PEL North Italy Joint Chapter since 2022. Since 2024, he has been an Associate Editor for IEEE TRANSACTIONS ON TRANSPORTATION ELECTRIFICATION. He was the recipient of five IEEE paper Awards and two IEEE Ph.D. thesis awards.

GAETANO DILEVRANO received the M.Sc. and Ph.D. degrees in electrical engineering from Politecnico di Torino, Turin, Italy, in 2020 and 2024, respectively.

He has been a Visitor with McMaster University, Hamilton, ON, Canada. He is currently with an international aerospace company as an Electric System and Motor Designer with a focus on more electric aircraft. His research interests include design and test procedures of electric motors and drives for electric and hybrid vehicle powertrains with emphasis on innovative electric machines, and the integration of machine and power converter and advanced test methodologies.

FAUSTO STELLA (Member, IEEE) received the bachelor's and master's degrees in electrical engineering and the Ph.D. degree in electrical, electronical and communication engineering from the Politecnico di Torino, Turin, Italy, in 2012, 2015, and 2019, respectively. In 2017, he was a visiting Ph.D. Student with the University of Nottingham, Nottingham, U.K.

He is currently an Assistant Professor with Politecnico di Torino, Turin, Italy. His research interests include the design of power electronic converters, focusing on SiC semiconductors and reliability issues, and the control of converters via embedded systems.

GIANMARIO PELLEGRINO (Fellow, IEEE) received the M.Sc. and Ph.D. degrees in electrical engineering from the Politecnico di Torino, Turin, Italy, in 1998 and 2002, respectively. He is currently a Professor of power converters, electrical machines, and drives with Politecnico di Torino, Turin, Italy. He was a Visiting Fellow with Aalborg University, Aalborg, Denmark, the University of Nottingham, Nottingham, U.K., and the University of Wisconsin–Madison, Madison, WI, USA. He initiated and leads the development of the open-source platform SyR-e for the design of electrical motors and drives, which is continually enhanced and validated through industry collaborations, and is widely adopted worldwide. He has coauthored more than 65 IEEE journal articles and holds nine patents.

Dr. Pellegrino is an Associate Editor for IEEE TRANSACTIONS ON INDUSTRY APPLICATIONS. He was the recipient of the 8th Grand Nagamori Award and nine best paper awards. He is a Founding Member of the Power Electronics Interdepartmental Center, Politecnico di Torino, serves on the Advisory Board of PCIM Europe, and is currently the Adjunct Vice Rector for Technology Transfer at Politecnico di Torino.

ALDO BOGLIETTI (Fellow, IEEE) was born in Rome, Italy in 1957. He received the Laurea degree in electrical engineering from the Politecnico di Torino, Turin, Italy, in 1981.

In 1984, he started his research work with the Department of Electrical Engineering, Politecnico di Torino, as a Researcher of electrical machines. In 1992, he was an Associate Professor of electrical machines and has been a Full Professor with Politecnico di Torino since November 2000. From 2003 to 2011, he was the Head of the Electrical Engineering Department, Politecnico of Torino. He is the author of more than 200 papers in the field of energetic problems in electrical machines and drives, high-efficiency industrial motor, magnetic material and their applications in electrical machines, electrical machine and drives models, and thermal problems in electrical machines.

Dr. Boglietti was the recipient of the ICEM International Conference on Electrical Machine Arthur Ellison Outstanding Achievement Award in 2020 and the Nikola Tesla Award 2024. He is the Past Chair of the Electrical Machine Committee of IEEE Industry Application Society and the Past Chair of the Electrical Machine Technical Committee of IEEE Industrial Electronic Society.